PHYSICAL REVIEW B **86**, 224403 (2012)

Dualism of the 5f electrons of the ferromagnetic superconductor UGe_2 as seen in magnetic, transport, and specific-heat data

R. Troć,* Z. Gajek, and A. Pikul

Institute of Low Temperature and Structure Research, Polish Academy of Sciences, P Nr 1410, 50-950 Wrocław 2, Poland

(Received 27 July 2012; revised manuscript received 15 November 2012; published 4 December 2012)

Single-crystalline UGe_2 was investigated by means of magnetic susceptibility, magnetization, electrical resistivity, magnetoresistivity, and specific-heat measurements, all carried out in wide temperature and magnetic-field ranges. An analysis of the obtained data points out the dual behavior of the 5f electrons in this compound, i.e., possessing simultaneously local and itinerant characters in two substates. The magnetic and thermal characteristics of the compound were modeled using the effective crystal field (CF) in the intermediate coupling scheme and initial parameters obtained in the angular overlap model. Various configurations of the localized $5f^n$ ($n = 1$, 2, and 3) electrons on the uranium ion have been probed. The best results were obtained for the $5f^2$ (U^{4+}) configuration. The CF parameters obtained in the paramagnetic region allowed us to reproduce satisfactorily the experimental findings in the whole temperature range including also the magnitude of the ordered magnetic moment of uranium at low temperature. The electrical resistivity data after subtraction of the phonon contribution reveal the presence of a Kondo-like interaction in UGe_2 supporting the idea of partial localization of the 5f electrons in UGe_2. On the other hand, magnetoresistivity and an excess of specific heat originated from the hybridized (itinerant) part of 5f states, apparent around the characteristic temperature T^*, give a distinct signature for the presence of the coupled charge-density wave and spin-density wave fluctuations over all the ferromagnetic region with a maximum at T^*, postulated earlier in the literature.

DOI: 10.1103/PhysRevB.86.224403 PACS number(s): 75.30.Gw, 71.23.An, 71.70.Ch

I. INTRODUCTION

The orthorhombic UGe_2 is treated by many authors as having ferromagnetic (FM) order ($T_C = 52$ K, $\mu_s = 1.4\mu_B$) due to itinerant U 5f electrons which are believed to form also the superconducting (SC) state under the pressure region of 1.0–1.6 GPa (see the vast review[1] and references therein). On this background such a coexistence has been a subject of several theoretical considerations (for literature see Refs. 2 and 3). The interplay of the SC/FM interactions has opened a number of speculations as to the formation of the unconventional SC state in this compound coexisting with a fairly strong FM ordering. However, the physics of UGe_2 even at zero pressure is still a matter of wide debates in the literature. Therefore, this initial point of consideration of the UGe_2 properties requires full clarification before going to the discussion of its properties studied under pressure.

In the past, the nature of the U 5f electrons was a subject of an intensive discussion in order to elucidate their different behaviors in a big variety of uranium compounds. Hence, the idea has arisen of coexisting 5f localized and itinerant states in some studied uranium or plutonium systems, which is known as dualism of 5f electrons. To explain this phenomenon, Zwicknagl and Fulde[4] developed theory for the electronic excitations in some uranium compounds which has been supported by a number of variety experiments, e.g., by photoemission and neutron inelastic-scattering measurements. Particularly in the case of UGe_2, it seems to be confirmed by muon-spin-relaxation studies (μSR) of Yaouanc *et al.* in their earlier works[5] and Sakarya *et al.* in recent[6] works. These authors, by presenting such a type of detailed investigations performed on single-crystalline UGe_2 at ambient and under pressure, respectively, have fully supported the above idea. In this scenario, UGe_2 has to be viewed schematically as a two-subset electronic system, where the localized 5f electrons are responsible for the ferromagnetic moment and huge magnetocrystalline anisotropy (MCA), while the itinerant electrons carry a small relative isotropic magnetic moment guaranteeing an unconventional SC. This leads to the fact that the bulk magnetic properties of UGe_2 mainly originate from the part of nearly localized 5f electrons being affected by crystalline-electric field (CF), but the other part of 5f electrons has also its obvious impact on the magnetic, thermal, and transport anomalous properties of this digermanide, but its signature is quite different from those of localized ones. Thus, such a view is presented in this paper, being in distinct contrast to those presented by other numerous authors who regard even now all the 5f electrons in UGe_2 at ambient pressure as being itinerant. It is worthwhile to underline here that the above dual role of 5f electrons we have also adopted to UGe_2 several years ago in our earlier various publications, cited below, concerning behavior of this interesting digermanide.

The discovery of superconductivity (SC) under pressure in the ferromagnetic UGe_2 (Ref. 7) is still associated with the observation of a broad anomaly in the temperature derivative of the resistivity having a diffuse maximum at the so-called characteristic temperature T^*, reported by Oomi *et al.*[8] An anomaly at T^* ($\sim 0.5T_C$), also was clearly detected in the coefficient of volume thermal expansion α_V (Ref. 9). Recently Kuwahara *et al.*[10] have found a very broad elastic anomaly related to T^* in the longitudinal c_{11} mode. This temperature at ambient pressure is reported to be between 25 and 30 K and it reaches zero just at the critical pressure $p_c^* \approx 1.2$ GPa, where T_{SC} (0.8 K) becomes the highest.[1,7] This anomaly presents rather some *crossover* than any phase transition, at least at low pressures. As a T^* anomaly origin, coupled charge- and spin-density wave (CDW-SDW) fluctuations were suggested.[11]

However, no satellite peak of the nesting origin was observed in neutron-diffraction measurements.[1] Also the linear coefficient $\alpha_V(T)$ at ambient pressure shows a broad hump at around $T^* = 25$ K.[12] Similarly a very broad huge negative minimum in the transverse magnetoresistivity (TMR), of the order of 40%, measured for the configuration $j \parallel b$ and $B \parallel a$, indicating the presence of very strong magnetic fluctuations around T^*, also was previously reported.[13] Until now, the nature of the characteristic temperature T^* has been a matter of intensive debate in the literature, but without any final conclusion.

Based on our data of the bulk magnetic, transport, and thermal properties[13–17] as well as band structure studies by electron-positron annihilation[18] and x-ray photoemission spectroscopy (XPS) measurements for UGe_2, also supported by up-to-date band-structure calculations,[19,20] we have discussed the anomalies of these different properties at T^* pointing out that their presence is due to the dualism of the $5f$ electrons in UGe_2, previously mentioned. Considering other mechanisms, but based on the itinerant character of all U $5f$ electrons in UGe_2, it was also proposed for example that the T^* anomaly is originated from the characteristic camel-shaped electronic density of states (DOS) with two peaks located very near E_F (Ref. 21) or represents a Stoner gap Δ of a perfect polarized state below T^*.[22] This gap in the heavy quasiparticle bands was estimated to be about 40 K at ambient pressure, and Δ was found to be decreasing monotonically with increasing pressure in a similar manner to that of the $T^*(p)$ dependence.[1]

Most of the works devoted to the coexistence of SC and FM in UGe_2 have been focused so far on the electronic and magnetic properties of this compound under pressure. It is a natural way to consider that the reason of the occurrence of SC in UGe_2 under pressure lies in its properties at ambient pressure. However, we think that the aforementioned arguments will allow us to receive a final acceptation of the point of view thus connected with the dualism model considered above in any future studies of UGe_2 at ambient pressure. It is well known that by applying pressure one can change the character of the $5f$ electron states and somewhat delocalize them, but this problem is out of our scope. A full recent account of physical properties of UGe_2 at zero and under pressure can be found in the muon work by Sakarya *et al.*,[6] already mentioned.

Below T_C the orthorhombic compound considered here shows strongly anisotropic magnetic behavior in its ferromagnetic state, characteristic of the f localized systems (as compounds based on the rare-earth elements). The experimental investigation performed by Sakon *et al.*[23] up to 27 T on a single-crystalline sample of UGe_2 and at atmospheric pressure has shown that this digermanide exhibits a giant magnetocrystalline anisotropy (MCA) field $B_a = 320(20)$ T at 4.2 K. In turn, the magnetocrystalline anisotropy constant $K_1 = 3.4$ kJ kg^{-1} measured at 4.2 K is a value comparable with that found for the most anisotropic rare-earth magnets. This fact probably leads to an unusually large gap in the magnon spectrum of UGe_2, hence we deal with an Ising-type ferromagnet. Due to this strong uniaxial MCA we do not expect to observe a conventional $M \sim T^{3/2}$ spin-wave-like dependence of magnetization M at low temperature.

In this paper, we present some magnetic, transport, and detailed thermodynamic investigations of UGe_2 and its nonmagnetic counterparts $ThGe_2$ and $ZrGe_2$, all performed at ambient pressure. Our specific-heat data obtained at zero and in high magnetic fields up to 5 T will be compared with those published very recently by Hardy *et al.*[24] who have presented detailed specific-heat and thermal-expansion measurements up to 8 T. We also report on the key role of the CF effect in understanding the magnetic and thermal properties of this digermanide. Moreover, we present here a consistent description of the electronic structure of U^{4+} ($5f^2$) ion in UGe_2, derived on the basis of the effective Hamiltonian calculations with the term mixing taken into account. In order to reduce the number of variable parameters, in an initial step we apply the angular overlap model approximation (AOM) (see Ref. 25 and references therein), but in the next step of our consideration of the CF parameters the AOM constraints are gradually removed. Thus the CF parameters refined in this way provide a final theoretical description of the temperature dependencies of anisotropic magnetic susceptibility and Schottky contribution to the specific heat of UGe_2 in its paramagnetic region.

II. EXPERIMENT

A single crystal of UGe_2 was grown by the Czochralski pulling method employing a tetra-arc furnace under protective atmosphere, as described earlier in Ref. 13. The measurements of susceptibility or magnetization of UGe_2 were made in a magnetic field of 0.5 T in the temperature range 1.9–300 K on a small oriented cubic lump with dimensions $3 \times 3 \times 3$ mm^3 which was cut from a big ingot of UGe_2 of about 4 mm in diameter and 40 mm in length. The quality of this material was verified by means of x-ray powder-diffraction measurements and microprobe analysis using an EDAX PV 9800 spectrometer.

The nonmagnetic reference counterparts of UGe_2, i.e., $ThGe_2$ or $ZrGe_2$, as polycrystalline samples, were obtained by arc melting the stoichiometric components under a titanium gettered argon atmosphere and then by annealing in vacuum at 800 °C for one week. The x-ray powder pattern showed in each case only one phase of the orthorhombic $ZrSi_2$ or $ZrGa_2$ types of structures with space groups *Cmcm* and *Cmmm*, respectively. The lattice parameters $a = 1.6624(5)$, $b = 0.4028(1)$, $c = 0.4146(1)$ nm for $ThGe_2$, and $a = 0.3816(1)$, $b = 1.5089(5)$, and $c = 0.3789(1)$ nm for $ZrGe_2$ were found. Any attempt to obtain the isostructural to UGe_2 phase, $ThGe_2$, i.e., of the $ZrGa_2$ type (space group *Cmmm*) has failed. The existence of the latter phase was previously reported by Brown[26] in his crystal refinement of both polymorphic types of $ThGe_2$ structures. As this author claims, it was impossible to form this phase in detectable amounts by arc melting and heat treating. However, he was able to obtain this phase as a very small single crystal, but not in a pure form, as a result of heating the Th-Ge alloys in liquid bismuth below 650 °C. Nevertheless, both $ThGe_2$ structures are closely related to each other and can be derived by a simple crystallographic translation.[26] Contrary to Brown's estimation, we do not find for our $ThGe_2$ phase any deficit in the Th component.

Magnetic susceptibility or magnetization measurements were performed in the temperature range 1.9–300 K. For these measurements we used a superconducting quantum interference device (SQUID) magnetometer. The electrical resistivity in zero field as well as in fields up to 5 T was measured in the temperature ranges 4.2–300 K and 4.2–80 K, respectively. We used a standard dc four-point technique and bar-shaped specimens of $1 \times 1 \times 5$ mm^3 dimensions. The heat capacity was measured in the temperature range from 4.2 K up to 300 K and in applied magnetic fields up to 5 T using a Quantum Design PPMS platform. The method of thermal relaxation[27] was applied. As a sample mounting medium Apiezon N vacuum grease was used.

III. Dual BEHAVIOR OF 5f ELECTRONS

A. Magnetic properties

The magnetization measurements on a single-crystalline sample of UGe_2 were performed by Menovsky *et al.*,[28] who found a huge anisotropic behavior with the easy magnetization along the a axis. Our later results on vast magnetic and electron transport measurements performed also on a single crystal of UGe_2 were already presented in two conference papers.[13,14] Our results, which showed the presence of extremely large anisotropy in the magnetic susceptibility and magnetization in this digermanide, confirmed the previous ones. There, we presented also the temperature dependence of the spontaneous magnetization for this compound, σ_s (in emu g^{-1}), inferred from the Arrot plot. The latter turned out to be consistent with that determined from neutron-diffraction measurements.[29] Here we show in Fig. 1, on enlarged scale, the temperature variation of the magnetization M (expressed in μ_B per U atom)

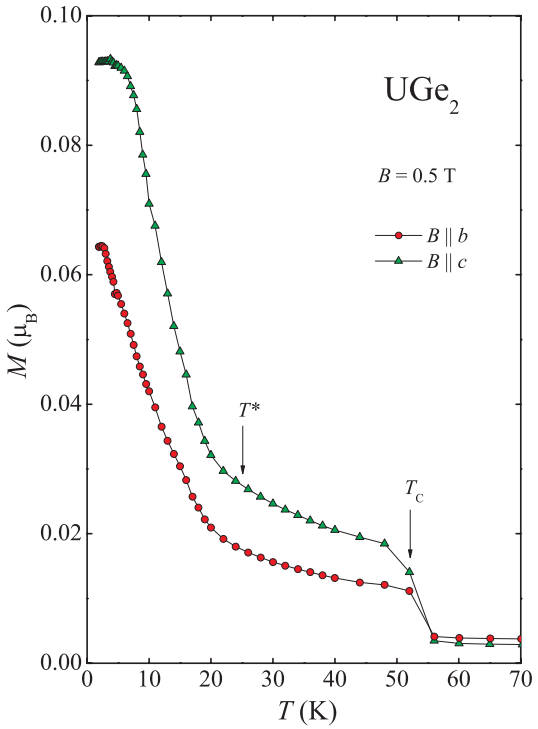

FIG. 1. (Color online) Magnetization of UGe_2 measured along two hard b and c axes as a function of temperature.

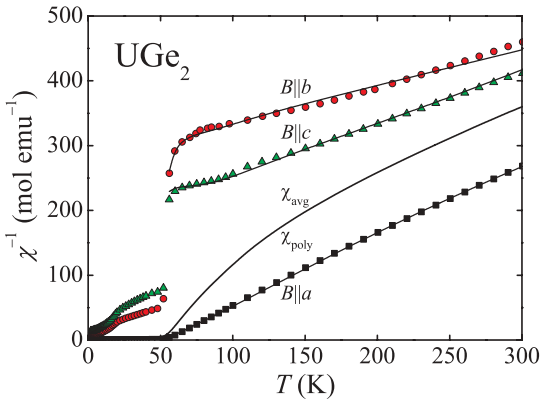

FIG. 2. (Color online) Experimental (points) and model (lines) inverse magnetic susceptibility for UGe_2 against temperature. The susceptibilities χ_{avg} and χ_{poly} converging into a single line are those averaged over the three field directions and measured on the polycrystalline sample, respectively.

performed for two hard directions, i.e., along the b and c axes in an applied magnetic field of 0.5 T. From this figure it is clear that thus along these hard magnetization directions one can distinctly observe a rapid but continuous variation of the slope in these two curves around the characteristic temperature T^*. Unfortunately, the preceding authors of Refs. 1 and 29 have measured the magnetization of UGe_2 only along the easy-magnetization axis a. So that they were not able to detect such an anomaly at T^* taking place along the hard directions. The latter observation seems to be a result of very small magnetization values of the order of $0.1\mu_B$ found along these hard directions at low temperature compared to that of the total one ($M_a \sim 1.4\mu_B$) found along the a axis. This anomaly certainly is connected with some change in the CDW-SDW fluctuations (see Ref. 11) below T^*, mentioned in the Introduction (Sec. I). Surprisingly, the $M_b(T)$ function for $B||b$ measured also by Sakon *et al.* and presented in Ref. 23 in Fig. 6 does not exhibit any anomaly in the vicinity of T^* and its low-temperature value is about only half of ours. A microscopic model of the coexistence of the FM and SDW phases has recently been considered by Hirohashi and Ueda[30] by taking account of the orbital degeneracy of the 5f electrons in UGe_2. In consequence, rich ground-state phase diagrams have been given.

The inverse susceptibilities of UGe_2 along the main crystallographic axes above T_C measured at zero pressure are displayed in Fig. 2. In accordance with previous such studies,[28,31,32] a large anisotropy in these dependencies is well apparent. The observed anisotropy, where $\chi_a \gg \chi_c > \chi_b$, is clear evidence that essentially the localized 5f electron states exist in UGe_2 and the CF effect is mainly responsible for this feature. The obtained magnetic characteristics by fitting the susceptibility to the modified Curie-Weiss (MCW) law are given in Refs. 13 and 14 in Table I. In Fig. 2 we present also two curves $\chi^{-1}_{avg}(T)$ (average of three directions) and $\chi^{-1}_{poly}(T)$ (results obtained on polycrystalline sample) which coincide, and hence we are sure of well performed measurements. It is clear that strong curvature in $\chi^{-1}_{poly}(T)$ illustrates the huge anisotropy in the magnetic behavior of UGe_2. Based on this conclusion we present below a CF approach yielding the

TABLE I. The MCW parameters for UGe_2 single crystal.

Axes	χ_0 (10^{-3}emu/mol)	θ_p (K)	μ_{eff} (μ_B)
a	0.43	53	2.60
b	0.38	−254	2.83
c	0.15	−200	3.02

crystal-field level scheme which explains well the observed large anisotropy and the temperature dependence in the magnetic susceptibility for this digermanide.

B. General description of the phenomenological approach

1. Structure and point symmetry

As we have already mentioned, UGe_2 crystallizes in the $ZrGa_2$ structure type (space group *Cmmm*) with large lattice ratios b/a and b/c of 3.76 and 3.68, respectively.[33] The uranium atoms are at positions $4j$ which have coordinates $(0, y_U, 1/2)$, where $y_U = 0.1415$. The U atoms form a zigzag chain propagating in the *a* direction with a nearest-neighbor U-U distance in the chain of 0.382 nm. The Ge atoms are located in the *ab* and *ac* planes at three positions: the Ge(1) atom at $4i$ has relative coordinates $(0, y_{Ge}, 0)$, where $y_{Ge} = 0.3084$, while the other two Ge(2) and Ge(3) atoms are at $2a$ and $2c$ positions, of relative coordinates (0,0,0) and (1/2,0,1/2), respectively. In this type of structure (considering the largest cell dimension along the *b* direction) the central atom U is surrounded by the eight nearest germanium atoms which form a distorted Archimedean antiprism [UGe_8] of approximately D_{4d} point symmetry, yielding the axial CF potential just along the *b* axis. The angles between the metal-ligand (ML) bonds differ, however, from those of ideal Archimedean antiprism by up to 20°. It is noteworthy that within the limits of experimental error this coordination in $ThGe_2$ with the space group *Cmcm* is only slightly different from that considered above.[26] However, because of the fact that the easy magnetization axis is along the *a* direction, in UGe_2 we had to choose just this axis as a quantized one. Then, after inclusion of two more distant germanium atoms Ge(1), the coordination around the U atoms changes into that shown in Fig. 3. As seen, this [UGe_{10}] coordination stands out with two slightly

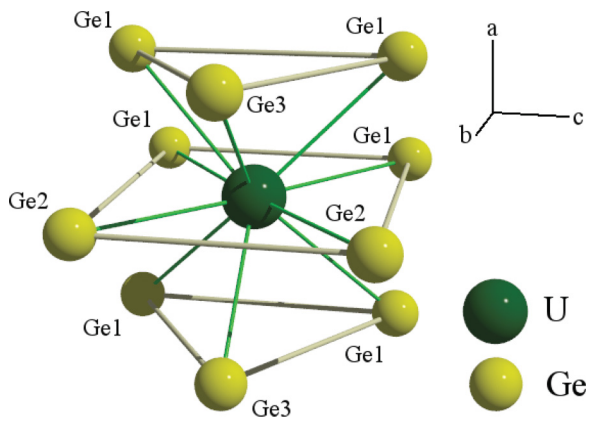

FIG. 3. (Color online) Coordination polyhedron of uranium atom in UGe_2 seen along the easy magnetization axis *a*.

deformed tetrahedra connected with vertices, separated by the coordination rectangle lying in the reflection plane.

2. Effective Hamiltonian of the localized electrons subsystem

The magnitude of the ordered and effective magnetic moments, temperature dependence of the magnetic susceptibility, and electronic contribution to the heat capacity suggest predominantly localized character of the $5f$ electrons in UGe_2 and point to the presence of the CF transitions. Therefore, we apply here the standard static description based on the renormalized Hamiltonian projected on the subspace of the pure f-electron states hoping that it is still capable of capturing the main features of the splitting of the $5f$ states despite the presence of the band electrons. Thus our effective Hamiltonian reads

$$H_{5f} = \sum_k F^k \hat{f}_k + \sum_i \zeta_{5f} \mathbf{l}_i \cdot \mathbf{s}_i + \sum_i \hat{h}_{CF}(\mathbf{r}_i/r_i) + \sum_i \mu_B(\mathbf{l}_i + 2\mathbf{s}_i) \cdot \mathbf{B}, \quad (1)$$

where i runs over the $5f$ electrons. The first two terms represent the so-called "free-ion" interactions of spherical symmetry: the Coulomb repulsion is conventionally parametrized with the Slater integrals F^k, $k = 2,4,6$ and the spin-orbit coupling tuned with the constant ζ_{5f}. The operators $\hat{f}_k$, $\mathbf{s}_i$, and $\mathbf{l}_i$ have their usual meaning. The above free-ion parameters have been fixed during the fittings. We use the values from Ref. 34 (see footnote [a] to Table II). The response of the system to external or internal (molecular) magnetic field **B** is represented by the Zeeman term in (1). The nonspherical part of the effective Hamiltonian—the CF potential h_{CF}—has the following form in Wybourne notation:[35]

$$\hat{h}_{CF}(\mathbf{r}/r) = \sum_{k,q} B_{kq} \hat{C}_q^{(k)}(\mathbf{r}/r), \quad (2)$$

TABLE II. The AOM geometrical coefficients W_{kq}^{μ} and two sets of the parameters B_{kq} (in K) obtained with and without the AOM constraints as described in the main text, in the coordinate system with $Z \parallel a$ and $Y \parallel b$. Values of the refined parameters transformed back to the crystallographic axes are given in the parentheses.

	W_{kq}^{μ}			B_{kq}	
kq	$\mu = 0$	$\mu = 1$	$\mu = 2$	AOM[ab]	Refined[ac]
20	−1.039	−1.716	0.000	1606	673(−1329)
22	−0.038	−0.091	0.000	58	−810(−7)
40	−0.522	−0.113	0.005	833	−5285(−7794)
42	1.001	0.346	−2.578	1841	2759(−1173)
44	−2.736	−0.967	7.496	−5631	−3472(−1373)
60	−3.411	5.313	−2.279	8792	11531(3676)
62	−0.646	1.017	−0.443	1681	2500(2800)
64	4.672	−7.152	2.983	−11849	−13615(−15714)
66	1.265	−2.131	1.026	−3510	−4077(−3632)

[a]The values of the Slater integrals and the spin-orbit coupling parameters were fixed at the following values (Ref. 34): $F^2 = 61\,376$ K, $F^4 = 56\,803$ K, $F^6 = 35\,176$ K, $\zeta = 2482$ K.
[b]The molecular field (MF) temperature shift θ_{CW} was fixed at the experimental value of the transition temperature, 52.5 K.
[c]The MF temperature shift θ_{CW} obtained in the fitting was somewhat higher than the transition temperature, namely, 54.02 K.

where $\hat{C}_q^{(k)}$ are the normalized spherical harmonics and B_{kq} are the CF parameters. In general for each $k = 2,4,6$, $q = -k, -k+1, \ldots, k$. Point symmetry reduces the number of the nonzero B_{kq} parameters in the symmetry-adapted coordinate axis system.[36] In the case of the group D_{4d} only three axial parameters B_{20}, B_{40}, and B_{60} remain in the coordinate axis system with the axis Z along the fourfold symmetry axis. Closer inspection of the coordination indicates that there are three various distances, namely 0.296, 0.294, and 0.291 nm corresponding to U-4Ge(1), U-2Ge(2), and U-2Ge(3), respectively. As will be seen below, these "imperfections" of the coordination polyhedron with respect to the approximate D_{4d} symmetry have proved to be enough to promote the nonaxial CF terms. Moreover, an inclusion into the enlarged coordination sphere of the two more distant ligands, namely U-2Ge(1) of 0.324, nm enhances the nonaxial terms even more. Therefore we keep the actual point symmetry of the uranium site, i.e., C_{2v}, [UGe_{10}] coordination polyhedron, and the coordinate system of the $Z \parallel a$ and $Y \parallel b$ axes. For this symmetry and coordinate system the summation in (2) is restricted to q positive and even and all the B_{kq} are real. There are nine such adjustable, independent B_{kq} parameters.

Below room temperature, due to an usual large CF splitting in the case of uranium compounds, only a few of the lowest CF levels manifest themselves clearly in the magnetic, thermal, and transport properties. The nine independent parameters of the effective CF Hamiltonian, $\hat{h}_{CF}$, are hardly determinable. To reduce this number we apply the angular overlap model (AOM)[37–40] at the beginning of our calculations. In this approximation the CF interaction matrix is parametrized in terms of only three so-called "intrinsic parameters" e_μ^t, where $\mu = 0\,(\sigma)\,,\ 1\,(\pi)\,,\ 2\,(\delta)$, and t labels the ligands. These AOM parameters relate to the ordinary CF parameters B_{kq} through the equation

$$B_{kq} = \sum_\mu W_{kq}^\mu e_\mu, \tag{3}$$

where e_μ are the weight mean values of e_μ^t averaged over the ligands. The W_{kq}^μ coefficients absorb all the information about the geometry of the coordination polyhedron (see Ref. 40 for further details). We use the crystallographic structure data presented in preceding subsection. For the quantization axis (Z) chosen towards the easy magnetization axis a, being perpendicular to the approximate C_4 of the idealized Archimedean antiprism, the nonaxial ($q \neq 0$) coordination factors $W_{kq\neq 0}^\mu$ become important. This is clearly seen in Table II, especially for the coordination factors with $q = 4$.

All the four interactions which form the effective H_{5f} (1) determining the properties of the localized 5f electron subsystem are diagonalized simultaneously in our calculations. The eigenvalues $E_{v,\alpha}$ and corresponding wave functions for given magnetic field B_α allow one to obtain the magnetic and thermal characteristics which can be fitted to the experimental data.

The molar magnetization $M_{\mathrm{mol},\alpha}$ for direction α is given by the expression

$$M_{\mathrm{mol},\alpha} = N_{\mathrm{A}} \frac{\sum_v \mu_{v,\alpha} \exp\left(-\beta E_{v,\alpha}\right)}{\sum_v \exp\left(-\beta E_{v,\alpha}\right)}, \tag{4}$$

where

$$\mu_{v,\alpha} = -\frac{\partial E_{v,\alpha}}{\partial B_\alpha} \tag{5}$$

and $E_{v,\alpha}$ are the eigenvalues of the Hamiltonian (1). The corresponding molar susceptibility can be calculated then simply by dividing the magnetization by external magnetic field:

$$\chi_{\mathrm{mol},\alpha} = \frac{M_{\mathrm{mol},\alpha}}{B_\alpha}. \tag{6}$$

3. *Crystal-field modeling*

We start with the AOM approximation. The exchange interaction above T_{C} is represented by molecular field (MF) shift λ or, equivalently, by θ_{CW} of the Van Vleck susceptibility along the axis of ordinates or the abscissa axis, respectively. The AOM parameters (or CF parameters in the next step) are fitted to the magnetic susceptibility in the paramagnetic phase in three directions as a function of temperature. We use the Levenberg-Marquardt method implemented by Schilder and Lueken computer programs.[41–44] The other details of the method have been presented elsewhere.[45]

The initial calculations have been performed for the three configurations $5f^n$, with $n = 1$–3 but only for $5f^2$ the fitting has converged with a reasonable accuracy. The intrinsic parameters obtained in this case are the following: $e_\sigma = -1617$ K, $e_\pi = 43$ K, $e_\delta = -1335$ K. The negative values and magnitudes might be surprising; nevertheless, for metallic systems an effective attractive interaction cannot be excluded. Such a contribution is generated among the others by the virtual bond state (VBS), the exchange interaction between the localized and band electrons, charge penetration, and higher-order renormalization terms. Moreover, the role of the particular mechanisms responsible for the effective attraction depends on the energy of the localized states with respect to the Fermi energy. We expect them to be more pronounced for the systems like UGe_2 for which, as we will see in Sec. III C, the Kondo screening takes place.

The B_{kq} parameters corresponding to the above AOM parameters through Eq. (3) are listed in Table II together with the final refined values obtained by direct fitting of all nine B_{kq} parameters. The former set has been used as the starting one in these final steps. Additionally, the MF temperature shift θ_{CW} has been allowed to vary during the fitting. The obtained value of 54.0 K being close to the initial one, $\theta_{\mathrm{CW}} = T_{\mathrm{C}} = 52.5$ K may be regarded as an additional confirmation of the stability of the obtained solution.

As Fig. 2 shows, the fit to the susceptibility data (solid lines) is very good. Note that the model restores both the strong anisotropy and shape of each of three curves except some larger deviation from experimental points observed for the weakest respond direction. We have checked that there is no other solution of similar quality. As seen from Table II, the refined values of B_{kq} differ from the approximate AOM results in the case of B_{40} and the second-rank parameters.

The latter parameters are relatively small in both the sets so their influence on the global structure of the eigenstates is rather moderate. On the other hand, just for $k = 2$ the AOM approximation is known to be the weakest one.[40] Taking into account both the above remarks the divergence observed

TABLE III. The electronic states of the localized electron subsystem obtained with refined parameters listed in Table II, grouped into singlets and doublets.

Irrep.	Energy (K)	$^3H_4$ components of the eigenstates[a]
$\Gamma_4^{(1)}$	0	$-0.4772\|^3H_{43}\rangle + 0.4772\|^3H_{4-3}\rangle - 0.4677\|^3H_{41}\rangle + 0.4677\|^3H_{4-1}\rangle$
$\Gamma_2^{(1)}$	5.8	$-0.6721\|^3H_{43}\rangle - 0.6721\|^3H_{4-3}\rangle$
$\Gamma_1^{(1)}$	128	$-0.7415\|^3H_{40}\rangle - 0.4067\|^3H_{44}\rangle - 0.4067\|^3H_{4-4}\rangle$
$\Gamma_4^{(2)}$	527	$-0.4517\|^3H_{41}\rangle\ 0.4517\|^3H_{4-1}\rangle\ 0.4447\|^3H_{43}\rangle - 0.4447\|^3H_{4-3}\rangle$
$\Gamma_3^{(1)}$	536	$0.4949\|^3H_{42}\rangle - 0.4949\|^3H_{4-2}\rangle\ 0.4161\|^3H_{44}\rangle - 0.4161\|^3H_{4-4}\rangle$
$\Gamma_3^{(2)}$	893	$0.4837\|^3H_{44}\rangle - 0.4837\|^3H_{4-4}\rangle - 0.4594\|^3H_{42}\rangle\ 0.4594\|^3H_{4-2}\rangle$
$\Gamma_1^{(2)}$	1328	$-0.4136\|^3H_{4-2}\rangle - 0.4136\|^3H_{42}\rangle - 0.3958\|^3H_{44}\rangle - 0.3958\|^3H_{4-4}\rangle\ 0.3739\|^3H_{40}\rangle$
$\Gamma_2^{(2)}$	1377	$-0.6250\|^3H_{41}\rangle - 0.6250\|^3H_{4-1}\rangle$
$\Gamma_1^{(3)}$	2863	$-0.4444\|^3H_{4-2}\rangle - 0.4444\|^3H_{42}\rangle - 0.3730\|^3H_{40}\rangle\ 0.3352\|^3H_{44}\rangle\ 0.3352\|^3H_{4-4}\rangle$

[a]The admixtures of the excited $^{2S+1}L_J$ terms (up to 20%), not shown.

for $k = 2$ is neither important nor surprising. However, the difference in B_{40} still remains puzzling and worrisome for the moment. Another interesting feature of the results gathered in Table II is the untypically high values of the parameters of rank 6 in both approaches. We see also that the refined set of parameters transformed back to the crystallographic axes (the values given in the parentheses) exhibits strongly axial character for $k = 2$ and 4, contrary to the parameters of rank 6, among which the tetragonal component B_{64} reaches as large a value as $-15\,714$ K. Apparently this unusual combination of parameters of various ranks makes the easy axis of the system perpendicular to the approximate D_{4d} axis.

The ground $^3H_4$ term (total spin $S = 1$, orbital momentum $L = 5$, and total momentum $J = 4$) contributes up to 80% in the nine singlets of the lowest energies in UGe_2, assuming the $5f^2$ configuration. The remaining components come from the excited $^{2S+1}L_J$ terms. These nine states have the following symmetries: three singlets Γ_1 and two singlets for each Γ_2, Γ_3, and Γ_4. The main, $^3H_{4M_J}, M_J = -4 \ldots 4$, components of the eigenstates obtained within the final, refined model are presented in Table III. As seen, the singlets are grouped so as to form three quasidoublets and three singlets characteristic of D_{4d} point symmetry. The quasidegenerate ground state $\Gamma_4^{(1)}, \Gamma_2^{(1)}$ allows the system to order magnetically just with the ordered moment of $1.51\mu_B$ along the easy axis a which has been calculated from the full wave functions, i.e., the main components listed in Table III supplemented with those not shown there, originating from higher, excited $^{2S+1}L_J$ terms. This value of the ordered moment nearly falls within the range 1.4–1.5μ_B/U_{at} of the experimental values known from the literature.

As we will show below in Sec. III D, also based on the above model Hamiltonian determined in the paramagnetic phase we have calculated the Schottky and molecular field contributions to the heat capacity in a wide temperature range covering both the paramagnetic and ordered phase. The Schottky contribution can be calculated using the formula

$$C_{\mathrm{Sch}}(T) = \frac{R}{T^2}\left[\frac{\sum_i E_i^2 e^{-E_i/T}}{\sum_i e^{-E_i/T}} - \left(\frac{\sum_i E_i e^{-E_i/T}}{\sum_i e^{-E_i/T}}\right)^2\right], \quad (7)$$

where summation runs over nine eigenvalues listed in Table III.

C. Electrical transport properties

Considering in the previous section that some part of $5f$ electrons in UGe_2 are mostly localized, one has to expect in this compound the presence of their interplay with the conduction electrons, which in consequence leads, e.g., to a Kondo-like behavior. It is then useful to express the measured $\rho(T)$ of a magnetic material as

$$\rho(T) = \rho_0 + \rho_{ph}(T) + \rho_m(T), \quad (8)$$

where ρ_0 is the residual resistivity (i.e., sample impurity and imperfections). The phonon term, $\rho_{ph}(T)$, of the electrical resistivity of a simple metal is often described by the Bloch-Grüneisen law, which predicts at low temperatures, where $T \ll \Theta_D$ (Debye temperature), a T^n ($n = 3$–5) behavior of the resistivity and its linear temperature dependence ($n = 1$) at higher temperature.

In order to determine the magnetic part, $\rho_m(T)$, we have used the classical method to separate the phonon contribution $\rho_{ph}(T)$ from the measured resistivity of UGe_2, by taking into account the electrical resistivity of the nonmagnetic, $ThGe_2$. As we have mentioned in Sec. II, this germanide, though being not isostructural with UGe_2, possesses the crystal structure very close to that of the latter compound. Thus, in Fig. 4 we display its temperature dependence of the resistivity,

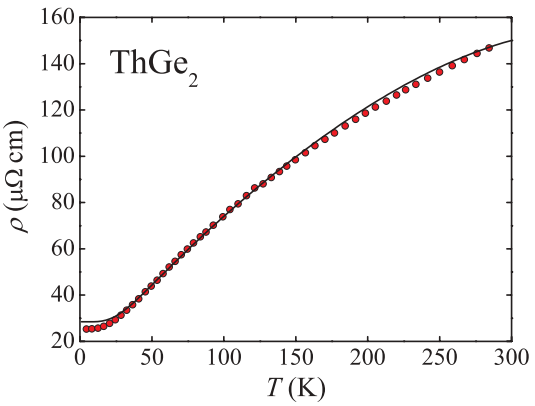

FIG. 4. (Color online) Temperature dependence of the resistivity of nonmagnetic $ThGe_2$. The solid line denotes the fitted BGM relation [Eq. (9)] pertaining to the phonon scattering.

$\rho(T) = \rho_0 + \rho_{ph}(T)$, which behaves as a typically metallic material, having a value of the residual resistivity ρ_0 of 25 $\mu\Omega$ cm. As shown in this figure (see the solid line), due to some downward curvature of $\rho(T)$ at high temperature we need to apply here the additional Mott interband scattering $s-d$ term, KT^3, to get a fairly good overall fit observed up to room temperature (RT). The obtained data were then fitted to the generalized Bloch-Grüneisen-Mott (BGM) relation,[46] given by Eq. (9):

$$\rho(T) = \rho_0 + 4R(T/\Theta_R)^n \int_0^{T/\Theta_R} \frac{z^n dz}{(e^z-1)(1-e^{-z})} - KT^3. \quad (9)$$

The second term was calculated with $n = 5$. R reflects the strengths of the electron-phonon interaction and its value is 0.354 $\mu\Omega$ cm K^{-1} while $\Theta_R = 160(5)$ K and $K = 1.4 \times 10^{-6}$ $\mu\Omega$ cm K^{-3}. The parameter Θ_R is usually considered to be close to the Debye temperature. All three of these terms yield the similar T variation as found for many other nonmagnetic intermetallic compounds, used as a phonon reference.

The temperature dependencies of the resistivity of single-crystalline UGe_2 were a subject of only a few works some years ago.[8,31] Only the a-axis resistivity was measured in the temperature range between 0.3 and 4.5 K and in magnetic fields up to 17.5 T, also applied along this axis.[47] The T^2 coefficient A of the resistivity was found to be 8 nΩ cm K^{-1} at zero field being then reduced by 50% with increasing field to 17.5 T. Results of our studies have been given in Ref. 14. For our values of A measured along three main directions see Table II of Ref. 14. That along the a axis is equal to 11 nΩ cm K^{-1}. From these latter studies it is also clear that the lowest resistivity we found at RT for j flowing along the easy magnetization axis a and the largest one for the most hard axis b. Interestingly that the resistivity value at RT measured along another hard axis c was not too much larger than that along the easy axis at this temperature. A similar tendency occurred also in earlier studies of other authors,[31] but with some differences in the residual resistivities and RT values. The mentioned differences in absolute values are less important when we analyze first of all the resistivities above $T_C = 52.5$ K, i.e., in the paramagnetic region. In Fig. 5 in the semilogarithmic scale the $\rho_m(T)$ is shown for the a and c axes after subtracting both features, namely the corresponding residual resistivities and the phonon contribution to the total measured resistivities along these two directions by applying the $ThGe_2$ reference.

The satisfactory fits of the experimental data to Eq. (10),

$$\rho_m(T) = \rho_0 + \rho_0^{\infty} + c_K \ln T, \quad (10)$$

found above 100 K in almost ideal logarithmic dependencies of $\rho_m(T)$ for these two directions, indicating the presence in UGe_2 of the Kondo lattice effect, are distinctly shown. The fitted parameters of $\rho_0 + \rho_0^{\infty}$ and c_K are shown in the figure. The observed deviation from this behavior and passing $\rho_m(T)$ by faint maxima before reaching T_C are the signature of the CF effect. It is clear now that UGe_2 is a case of the coexistence of the FM and combined CF and Kondo lattice effects. However, such a coexistence for a long time has been regarded as being in a strong conflict, whereas at present this is quite possible owing to the recently developed theory. This is the

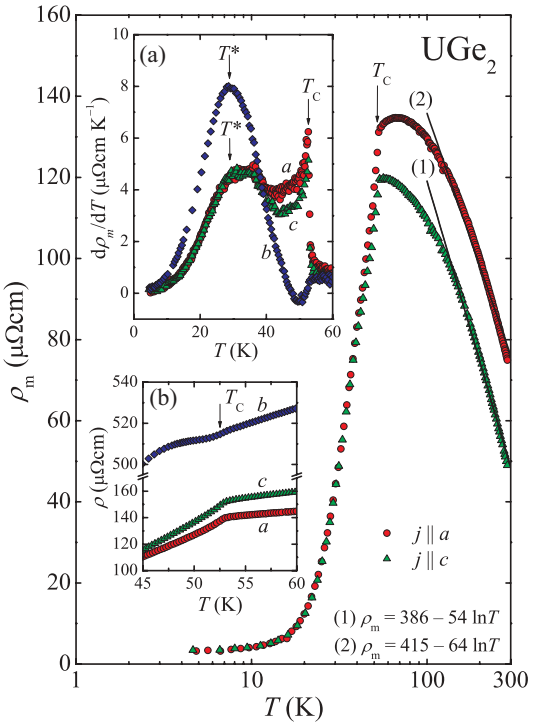

FIG. 5. (Color online) Temperature dependencies of the electrical resistivity measured for $j \parallel a$ and c after subtracting the phonon contribution, Solid lines are the best fits to Eq. (10). Insets: (a) Temperature dependence of the resistivity derivatives. (b) $\rho(T)$ behavior around T_C. For both cases it is shown for all the three main crystallographic directions.

so-called underscreening Kondo lattice (UKL) theory which has just been successfully applied to a number of uranium or neptunium compounds.[48] To this family of various actinide compounds the UCu_2Si_2 ferromagnet also belongs, which very recently has been deeply studied.[49] In turn, the extracted $\rho_m(T)$ from experimental $\rho(T)$, but measured for $j \parallel b$, behaves in another way. Above T_C this first goes through a wide maximum at about 150 K but its logarithmic thermal variation is observed only above 190 K (see Fig. 5 in Ref. 17). In the upper inset to Fig. 5 we present the temperature derivatives of the resistivity, $d\rho_m(T)/dT$, for all three main crystallographic directions. It is observed that if the very sharp peaks in $d\rho_m(T)/dT$ vs T dependence, determining T_C, are at the same temperature for all three of these directions, both the temperatures of the diffuse maximum describing the characteristic temperature T^* and their values (amplitudes) at this temperature are somewhat different for the b direction. It appears that T^* determined for this direction is found at slightly lower temperature and having almost a double amplitude larger at T^* than those for the a and c axes. Certainly this observation has some connection with the anisotropy of the FS.[19] In turn, in the lower inset of Fig. 5 we have plotted the $\rho(T)$ behavior for a,b, and c axes, just around the T_C temperature. As seen from this inset, the Curie temperature is 52.5 K and a *hump* of Cr-like shape occurs just below this critical temperature, but only along the b axis. This hump was recorded by Ōnuki *et al.*[31] and then in our measurements.[13,14] However, for the purpose to understand another face of the 5f electron dualism, i.e., the subsystem

being more itinerant, the transverse magnetoresistance (TMR) results found for UGe_2 have to be described here, in what follows below.

The main problem arising in explanation of the appearance of SC in the ferromagnetic state of UGe_2 under pressure is attributed to the nature of the pressure dependence of the characteristic temperature $T^*(p)$. It seems that up to now there exist no definite, microscopic explanation of this temperature and its pressure dependence at least in the low-pressure range. Elastic neutron scattering under pressure up to 1.6 GPa and down to 60 mK found no change in Bragg peak intensities or in their width through the SC transition temperature T_{SC} (0.7 K).[50] This fact indicates substantially that the FM of UGe_2 is not affected by the onset of the SC under pressure. This conclusion underlines strongly the fact that in UGe_2 the $5f$-electron two subsystems are almost independent of each other. This aspect remains to be accounted for by any future theory which should emphasize the FM/SC coexistence rather than their competition. It seems that thus taking into account an idea of the above two subsystems is here very helpful.

Only one study exists in the literature for UGe_2, where the TMR [defined as $\Delta\rho/\rho_0 = [\rho(B) - \rho(0)]/\rho(0)$], and measured for a configuration $j \parallel a$ and $B \parallel b$, was done at 4.2 K under pressures up to 2 GPa and in magnetic fields up to 5 T.[51] For this configuration $\Delta\rho/\rho_0$ achieves as large a positive value as about 60% at zero pressure and 5 T. An application of pressure decreases this value down to 10% at 1.5 GPa. This large positive value found at low temperature confirms the earlier corresponding TMR study of Ōnuki *et al.*,[52] carried out only in zero pressure and at 0.5 K, but for all the possible configurations. Unexpectedly for a ferromagnet, in all these cases $\Delta\rho/\rho_0$ turns out to be highly positive at this low temperature. From these results it was concluded that the open orbits exist along the b and a axes. In turn, we have made the zero-pressure complete TMR studies for a UGe_2 single crystal in the ferromagnetic region of temperatures, applying the magnetic fields up to 8 T and for j flowing along the three main directions.[13,14,53] In Fig. 6 we display here only the results of TMR obtained for one configuration, i.e., $j \parallel b$ and $B \parallel a$ at 1, 3, 5, and 8 T, for which the value of $\Delta\rho/\rho_0$ reaches at T^* (=27 K) a huge value of 40% at $\mu_0 H = 8$ T. Among a great deal of various data obtained so far for this digermanide, this result seems to be one of the most important. We connect this giant effect of magnetic field on the resistivity just around $T^*(\approx T_C/2)$ with freezing out strong magnetic fluctuations which, however, exist in the whole range of temperatures of the ferromagnetic order.

Our TMR data are in full agreement with the muon-spin-relaxation ones.[5,6] As the authors of these papers claim, the detected fluctuations do not arise from the localized uranium $5f$ electrons, but both subsets are found simultaneously at a single temperature T_C, whereas for UCu_5 and UPd_2Al_3 the temperatures at which the two subsets are detected are far apart. This highly suggests that freezing these fluctuations by pressure as indicated by the TMR studies of Ref. 51 made under pressures (mentioned above), i.e., close to the critical point p_c^* ($\approx$1.2 GPa) where T^* is close to 0 K. Hence, the low-energy fluctuations associated with p_c^* play a significant role in forming the SC state in UGe_2, which we postulated about ten years ago.[54] This conclusion was

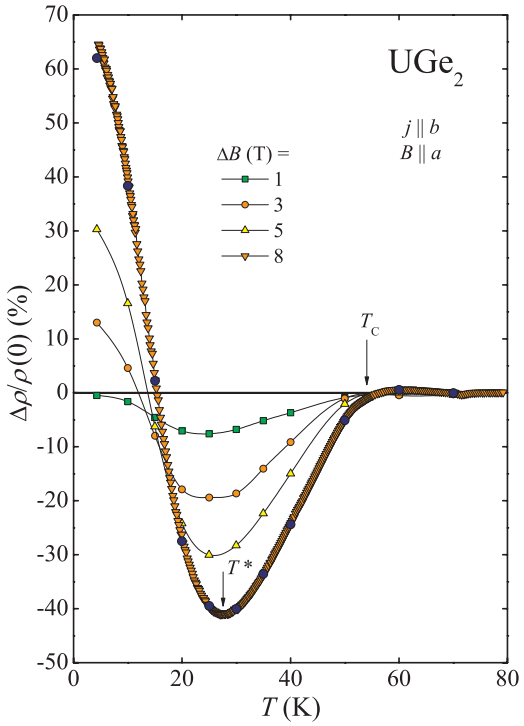

FIG. 6. (Color online) The TMR measured for the configuration $j \parallel b$ and $B \parallel a$ taken at various temperatures and in fields up to 8 T. The closed blue circles are the $\Delta\rho/\rho_0$ values found from their dependencies on an applied magnetic field at 8 T (see Fig. 5 in Ref. 53).

based on the magnetoresistivity experiments made on the polycrystalline sample of this compound. Coming back to our MR measurements on a UGe_2 single crystal, it is interesting to note (see Fig. 6) that we do not observe at all any simple critical ferromagnetic fluctuations of the magnetic moments at T_C just for the coordination considered here, though such type of fluctuation is well observed for the other configurations of TMR (see Ref. 53) measured by us. As is also seen in Fig. 6, TMR measured at 4.2 K and in fields above about 3 T becomes highly positive in accordance with the results of earlier works.[51,52] Summing the above discussion, one sees that a strong anisotropy occurs in UGe_2 not only in the magnetic properties, but also in the transport ones, i.e., in the resistivity,[13,31] TMR,[50] Hall effect,[15] and thermal conductivity.[17]

D. Heat capacity in magnetic fields

Usually the heat capacity, $C_p(T)$, for magnetically ordered uranium compounds involves several different contributions which can be presented as a sum:

$$C_p(T) = C_{el} + C_{ph} + C_{mag}, \tag{11}$$

where C_{el}, C_{ph}, and C_{mag} are the electronic, electron-phonon, and magnetic parts of the total heat capacity measured, respectively. In turn, the components of the latter contribution C_{mag} usually are considered to be also a sum of C_m (connected with the λ anomaly of a magnetic order), C_{Sch} (attributed to the Schottky anomaly), and C_K (Kondo specific heat) contents. In analyzing all these contributions, the most important need

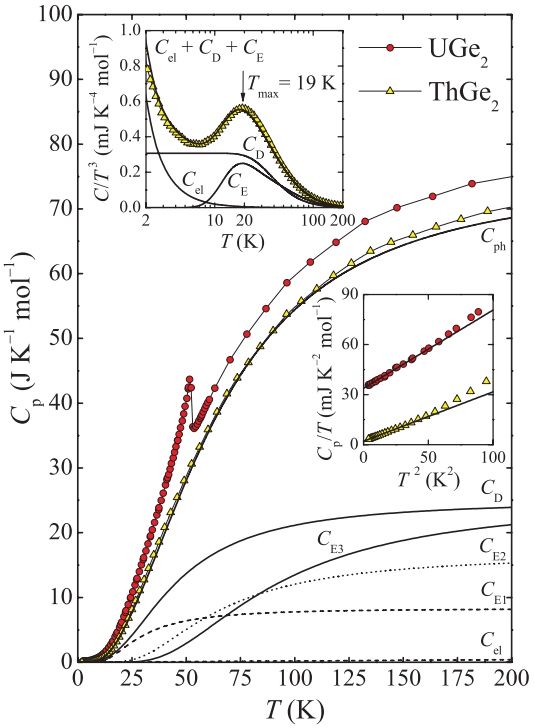

FIG. 7. (Color online) Experimental heat capacities of UGe_2 and nonmagnetic $ThGe_2$. The latter diminished by its C_{el} is taken as $C_{ph}(T)$ part of the total heat capacity of UGe_2. There are also shown all the particular contributions of the decomposed $C_{ph}(T)$ curve. The thick solid curve indicates their fitting sum. The lower-right inset shows the C_p/T vs T^2 low-temperature behavior for UGe_2 and $ThGe_2$, whereas the upper-left inset illustrates all the derived contributions to the electronic and phonon parts by means of the C_p/T^3 vs ln$T$ dependence.

is, however, a finding of a realistic phonon heat-capacity contribution, i.e., to determine a shape of the C_{ph} vs T curve as accurately as possible. As shown below, to do this we use the heat capacity of a reference nonmagnetic material. Other attempts to find $C_{ph}(T)$, described in the literature, lead often to erroneous final numerical results and conclusions, which makes them quite invalid. It could be done the best by using neutrons. However, in practice it does not work well because of the difficulty to get accurate low-energy transfers.

The previous zero-field heat-capacity curve C_p (solid line) of Ref. 27 measured for UGe_2 agrees quite well with our data (red closed circles) presented in Fig. 7 and measured up to 200 K. The ferromagnetic transition manifests itself by the λ-shaped anomaly at $T_C = 52.5$ K. In the upper-left inset to this figure there are shown the low-temperature plots, C_p/T vs T^2, for UGe_2 and $ThGe_2$, which extrapolated to $T = 0$ K yield the coefficients of the electronic heat capacity $\gamma(0)$ equal to 33 and 2 mJ/mol K^2, respectively. The low-temperature Debye constants Θ_D^{LT} are 232 and 240 K, respectively. These parameters for $ZrGe_2$ are $\gamma(0) = 3.5$ mJ/mol K^2 and $\Theta_D^{LT} =$ 310 K. In our analysis of the sum of magnetic and electronic terms ($C_{mag} + C_{el}$) for UGe_2 it was assumed that $C_{ph}(T)$ of UGe_2 can be derived from $C_p(T)$ of $ThGe_2$ by subtracting from the latter its C_{el}. In the same figure, we have plotted also the experimental points for $ThGe_2$ (open triangles).

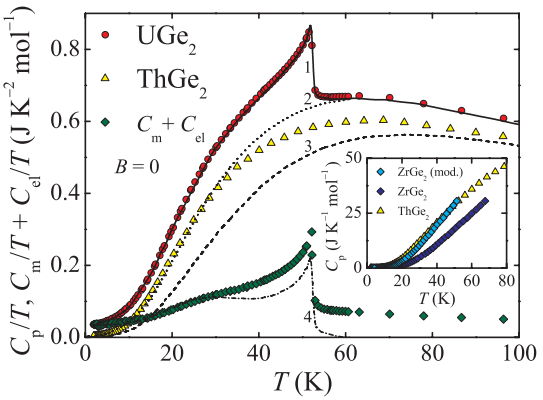

FIG. 8. (Color online) The C_p/T vs T plots of experimental data of UGe_2 and $ThGe_2$. In addition, curves 1 and 2 as well as 3 denote the heat capacity divided by temperature reported in Refs. 24 and 56, respectively. Also shown are C_{mag}/T together with C_{el}/T both vs T curves separated from the total heat capacity in the present paper (diamonds) compared to those taken from Ref. 24 (dot-dashed curve).

In order to get information about the possible presence also of the optic modes in $C_{ph}(T)$ of $ThGe_2$ we have plotted in the lower-right inset of Fig. 7 the C/T^3 vs ln$T$ function which goes through a maximum at $T_{max} = 19$ K. Thus this temperature multiplied by 5 gives rise to the C_{E1} mode characterized by the Einstein temperature $\Theta_{E1} = 95$ K. Almost the same T_{max} (= 20 K) was reported by Lashley *et al.*,[55] analyzing in a similar manner the above function, but directly for UGe_2. However, for a compound having $n = 3$ atoms per unit formula, we have to do with three acoustical and $3n - 3$ optical modes. We were able to find the remaining contributions by best fitting their sum to the experimental results. Thus the obtained smooth curve (thick line) may be described by the formula composed from five terms:

$$C_p(T) = C_D + C_{E1} + C_{E2} + C_{E3} + C_{el}. \qquad (12)$$

In this formula, the acoustical phonons are connected mainly with the heavier atom of Th (U) and can be simply described by three Debye modes (C_D) with the average Debye temperature $\Theta_D = 185$ K. The optical phonons connected with the two lighter Ge atoms are represented by six Einstein modes with the characteristic temperatures Θ_{E1}, Θ_{E2}, and Θ_{E3} being equal to 95, 200, and 280 K and with 1, 2, and 3 modes, respectively. As seen, the above fit though being fairly good at low temperatures shows, however, some poorer agreement with the experiment at higher temperature. A similar fitting we have made for $ZrGe_2$ and we found the following parameters: $\Theta_D = 305$ K, $\Theta_{E1} = 150$ K, and $\Theta_{E2} = 300$ K with 3, 2, and 4 modes, respectively.

In a previous paper by Hardy *et al.*,[24] the lattice heat capacity of UGe_2 has been decomposed into a single Debye function $C_D(T)$ and two Einstein terms $C_{E1}(T)$ and $C_{E2}(T)$ which reproduced their model based on the mean-field procedure of subtracting $C_{MFA}(T)$ from the total heat capacities $C_H(T)$ measured in magnetic fields up to 8 T (for details see Ref. 24). To illustrate the problem of subtraction of the phonon part from measured data to get the magnetic and electronic part, $C_{mag}(T)$, but with using several different phonon approaches, we present in Fig. 8 of three such cases. So that in this

figure apart from the form of C_p/T vs T curves used to experimental data of UGe_2, i.e., ours (closed red circles) and those from Ref. 24 (no. 1), which fully coincide, as well as our data for $ThGe_2$ (closed yellow triangles), we have also plotted the phonon reference results taken from Ref. 24 (no. 2) and inelastic neutron-scattering results of Ref. 56 (no. 3) as well.

Due to considerably smaller overall magnitudes of the $C_{ph}(T)$ function found from neutron studies (curve 3), any use of this curve as the phonon reference may be regarded as groundless. Hence, this also yields too high magnetic entropy at T_C, equal to $1.51R\ln 2$. As even the authors of this paper themselves claim, the large number of phonon branches preclude any meaningful modeling of the data. Also the applying as a phonon contribution, shown in Fig. 8 as curve 2, seems not to be quite appropriate at least above 30 K. The latter approximation results in an abrupt fall of C_m/T vs T function at T_C (neglecting C_{el}) and its tendency to zero at a little higher temperature, as is also demonstrated in Fig. 8 by the dot-dashed curve 4, compared to our approach marked by diamond experimental points. Such a coincidence with the $C_p(T)$ curve just above T_C not only leads to lowering the magnetic entropy magnitude, S_{mag}, but is also unable to manifest other features taking place in the paramagnetic state described below. The latter can be disclosed only by using some suitable nonmagnetic reference material with similar molar mass as the studied compound. As we have already mentioned, the crystal structure used in this study, $ThGe_2$, differs only slightly from that of UGe_2 [in unit-cell volume only by 5% (Ref. 26)]. In order to prove that there is no significant difference between $C_{ph}(T)$ of $ZrGe_2$ renormalized by existing difference in the molar mass and that found for $ThGe_2$ we carried out the so-called corresponding-states calculation where

$$C_{ph}(\mathrm{ThGe_2},T) = C_{ph}(\mathrm{ZrGe_2},kT), \quad \text{here}$$
$$k \approx \Theta_D^{LT}(\mathrm{ThGe_2})/\Theta_D^{LT}(\mathrm{ZrGe_2}) = 240/310 = 0.77. \quad (13)$$

The coefficient k has been calculated also on the basis of the Bouvier *et al.*[57] equation:

$$k = \sqrt[3]{\frac{M_{\mathrm{Zr}}^{3/2} + 2M_{\mathrm{Ge}}^{3/2}}{M_{\mathrm{Th}}^{3/2} + 2M_{\mathrm{Ge}}^{3/2}}} \approx 0.76, \quad (14)$$

where M is a given molar mass. This equation is valid rather only at low temperatures (for discussion see Ref. 57). The inset to Fig. 8 just displays $C_p(T)$ modified by coefficient k derived for $ZrGe_2$ being isostructural to UGe_2, which is further compared to the measured $C_p(T)$ of $ThGe_2$. The very small difference in these two nearly superimposed onto each other functions supports our assumption that the latter function determined for $ThGe_2$ can be used properly as the phonon reference studied here by us, UGe_2.

Next, we analyze the extracted C_{mag} vs T curve of UGe_2 containing also the electronic part C_{el} given in Fig. 9 in the whole region of measured temperatures. In the inset to this figure, we display the CF level splitting scheme with degeneracies and energies given in Table II. Thus, this scheme and energies have been used to calculate the Schottky heat capacity, C_{Sch}, in the paramagnetic region by applying Eq. (7).

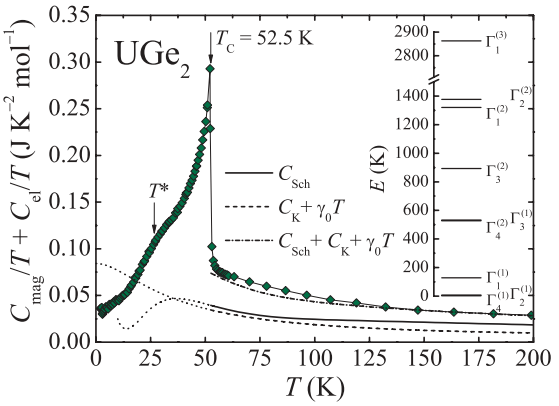

FIG. 9. (Color online) The $(C_{mag}/T + C_{el}/T)$ vs T plot. A λ-type anomaly at T_C and a hump at T^* found within the ferromagnetic region. The excess of heat capacity in the paramagnetic region originates from the Schottky anomaly (C_{Sch}/T) and Kondo effect (C_K/T) in UGe_2. The conduction electron heat capacity has also been included.

This contribution is shown by means of a thick solid curve above T_C and by a dot curve below this critical temperature. Apart from this CF contribution, we expect to deal here also with some Kondo-type contribution as an excess of heat capacity, C_K, in the paramagnetic region. According to Schotte and Schotte,[58] the Kondo-impurity contribution C_K to the total specific heat of 1 mol of the impurities with an effective spin $S = 1/2$ can be described by the formula

$$C_K\left(\frac{T}{T_K}\right) = 2R\frac{T_K}{2\pi T}\left[1 - \frac{T_K}{2\pi T}\psi'\left(\frac{1}{2} - \frac{T_K}{2\pi T}\right)\right], \quad (15)$$

where R is the universal gas constant, ψ' is the first derivative of the digamma function, and T_K is the Kondo temperature of the system, defined as the width of the Lorentzian-shaped Kondo resonance at the Fermi level. Figure 9, among others, displays also the so-obtained Kondo heat capacity C_K, divided by temperature T, for $T_K = 110$ K. Additionally, we add the heat capacity of conduction-band electrons represented by the term $\gamma_0 T$ with γ_0 of 5Å mJ/mol K^2 because that at $T =$ 0 K, given above, certainly decreases rapidly with increasing temperature and in the paramagnetic region becomes rather small. In Fig. 9 the Kondo heat capacity contribution is displayed by the long-dashed line at temperatures above T_C, but below this temperature, i.e., in the ordered state, C_K/T of UGe_2 reaches by extrapolation to $T = 0$ K even a value of about 80 mJ/mol K^2 (see the short-dashed line). It is highly probable that the ferromagnetism just depresses this value down to 33 mJ/mol K^2, as measured. Summing up all these contributions in the paramagnetic region, we obtained the dot-dashed line in Fig. 9. Some apparent remaining tail can be short-range magnetic order.

In Fig. 10 we have plotted only the magnetic and electronic parts, i.e., $(C_m/T + C_{el}/T)$ vs T at zero-magnetic field to analyze the hump at T^* (=27 K) and to determine the magnetic entropy, S_m, at T_C. To achieve this point we first of all have to fit the C_m/T experimental results to some formula (rather more appropriate for an Ising system than describing that as spin-wave behavior) well covering the C_m/T data up to temperatures close to T_C, with a purpose to extract the hump.

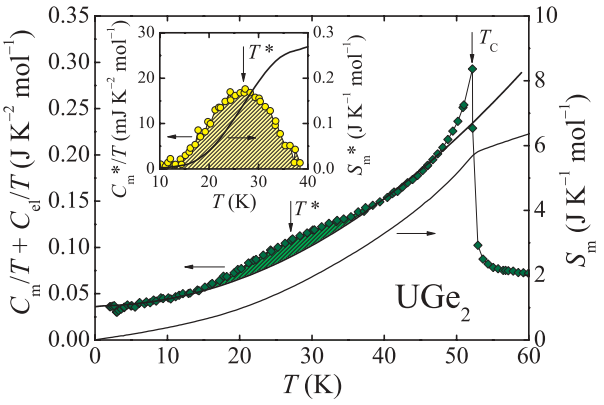

FIG. 10. (Color online) Fitting curve of the magnetic and electronic heat capacity divided by T and magnetic entropy both being dependent on temperature. The inset shows the extracted part of the hump in a manner of its C_m^*/T vs T and $S_m^*(T)$ dependencies.

The formula fulfilling this condition is as follows:

$$C_m(T)/T = \gamma(0) + aT^2\exp(-\Delta/T), \tag{16}$$

where $a = 7.0(3)10^{-5}$ J/mol K^2 and $\Delta \approx 0$ K. Thus, this formula describes the temperature dependence of heat capacity divided by T, simulating magnons in UGe_2. As seen from Fig. 10, a very good agreement with experimental points until several degrees below T_C (= 52.5 K) has been achieved. The same relation corresponding to the Fermi-liquid theory has been found for a ferromagnet URhSi.[59]

As is clear from Fig. 10, the magnitude of S_m at T_C for UGe_2 is equal to $R\ln 2$ (5.76 J/mol K) which is expected for the ground pseudodoublet of two CF levels very close in energy, presented in Table II. This value obtained by us stands in opposition to the corresponding literature data of 4.61 (Ref. 24) and 8.7 (Ref. 54) by taking into account in the latter case the neutron data for phonons. The magnetic entropy S_m^* of the hump is very small accounting only 0.28 J/mol K at 40 K. This fact fully supports the muon-spin-rotation (μSR) measurements.[5,6] On their basis, it has been pointed out that in UGe_2 there exist at ambient pressure itinerant long-range magnetic correlations with very small magnetic moment of $0.02\mu_B$. These correlations are characterized by long-wavelength magnetic fluctuations of a MHz range which are a signature of bandlike electrons. A similar value of the magnetic moment for the conduction electrons was found in the analysis of polarized neutron scattering.[29] This picture presented for UGe_2 in the present work and based on its macroscopic properties and that reported above but based on microscopic μSR data is quite different from that given by Hardy *et al.*[24] These authors at ambient condition of UGe_2 divide their zero-field magnetic heat capacity and magnetic thermal-expansion data into two comparable contributions related to two different ferromagnetic phases, namely FM1 and FM2 (for details see Ref. 24). They also demonstrated that the magnetic heat capacity, C_{MFA}, calculated in the molecular field approximation (MFA) and associated with the diffused maximum at T^*, follows the Stoner theory. Hence they treated their ferromagnetic low-temperature phase FM2

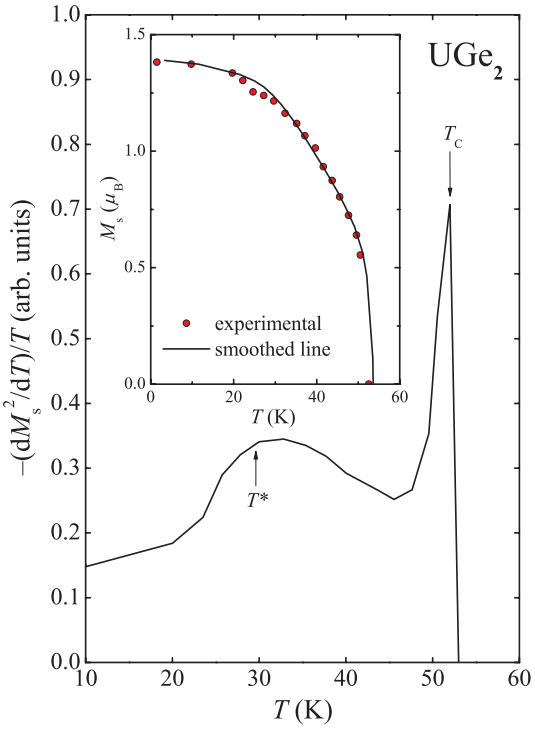

FIG. 11. (Color online) Magnetic heat capacity simulated only by the function $(dM_s^2/dT)/T$ vs T. The inset shows the determined spontaneous magnetization, M_s vs T, as reported in Ref. 14. The derivative was calculated from the smoothed curve determined through the experimental points (solid line).

as being itinerant. Since the thermodynamic relation

$$C_m(T) \sim \frac{dM_s^2}{dT}, \tag{17}$$

where M_S is here the spontaneous magnetization, is well known, we have differentiated our smoothed spontaneous magnetization data based on our measurements of $M_S(T)$ (taken from Ref. 14), which is also given in the inset of Fig. 11. Considering only the derivative of Eq. (17) divided by T, as a result we have obtained a similar behavior as those discussed above by Hardy *et al.* who used in this purpose only the magnetization curves taken in external magnetic fields up to 8 T. From this fact we conclude that the observed somehow puzzling $C_m(T)$ behavior of UGe_2, i.e., exhibiting the hump at T^* and sharp peak at T_C, does not lie in itinerancy of 5f electrons of the FM2 phase, but first of all in the shape of the temperature variation of M_S which reflects two electron subsets, i.e., the strong localized and very tiny itinerant ones. It is easy to demonstrate that a subtle change in the $M_S(T)$ curve brings about a large temperature variation in the discussed derivative divided by T. In other words, the bandlike feature studied by μSR experiment could be revealed by using solely relation (17), apart from any content of the coefficient of proportionality in the Stoner or Weiss models. On the other hand, the M_S vs T curve of UGe_2, despite its giant magnetocrystalline anisotropy, behaves rather as that based on the molecular-field theory in contrast to that expected for an Ising system [see, e.g., such a behavior in $DyPO_4$ (Ref. 60)].

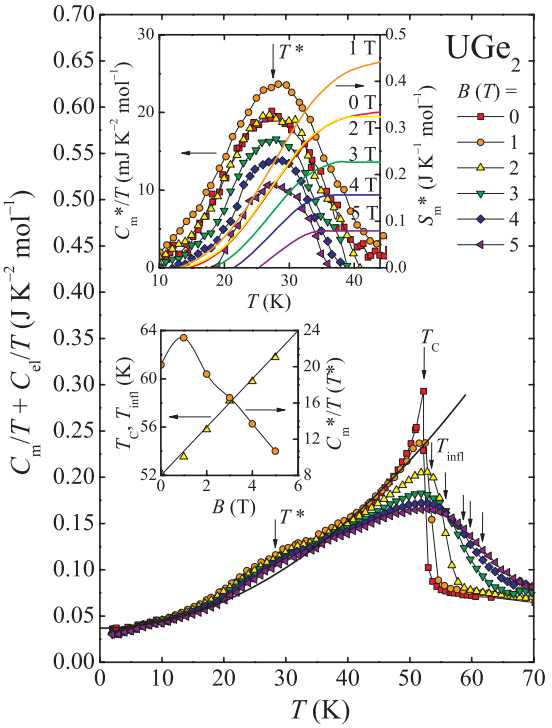

FIG. 12. (Color online) Magnetic heat capacity, C_m/T, together with the electronic one, C_{el}/T, as a function of temperature measured under applied magnetic fields up to 5 T. The solid line presents Eq. (16). Upper inset shows the extracted humps and their magnetic heat capacity divided by temperature, $C^*_m(T)/T$, and entropy, $S^*_m(T)$, for each hump measured at 0, 1, 2, 3, 4, and 5 T. Lower inset displays the magnetic-field variation of $C^*_m(T)/T$ at T^* (=27 K). There is also plotted T_C or T_{infl} as a function of magnetic field.

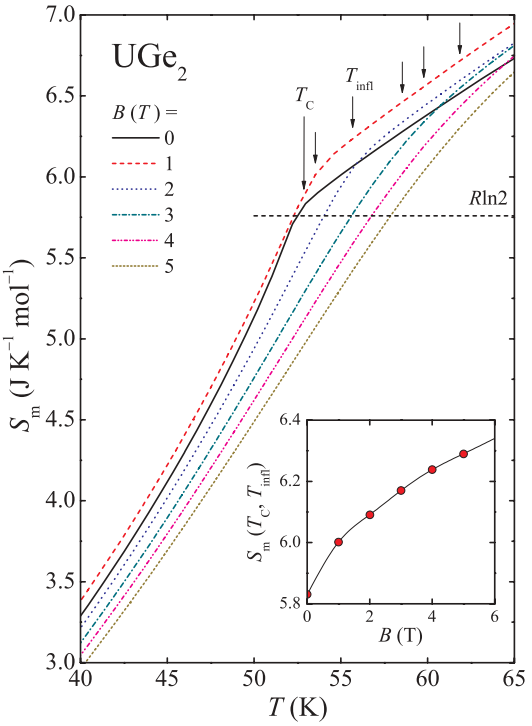

FIG. 13. (Color online) Increase of the magnetic entropy S_m accompanied with an applying of magnetic field. The arrows point out the characteristic temperatures T_C or T_{infl}. The inset indicates the growing magnetic entropy at the transition points under the magnetic field.

Furthermore, Fig. 12 illustrates the evolution of the heat capacity of UGe_2 upon applying an external magnetic field. The data were taken upon cooling in a magnetic field applied along the easy magnetization a axis. As seen, the λ-shaped peak determined at zero field starts to diminish continuously, more and more broadening with increasing magnetic-field strengths and its inflection point, T_{infl} (taken as a signature of the transition point) shifts towards higher temperatures. Thus, such a behavior of $C_m(T)$ in a magnetic field is characteristic of ferromagnets. Contrary to Lashley *et al.*,[55] such a behavior is just expected for the localized ferromagnetic systems (see, e.g., Refs. 61–63). As shown in the lower inset, this increase in T_{infl} is linear while the magnitude of the peak of the hump at T^* initially grows (maybe erroneously) and then diminishes rapidly with the strengths of magnetic field. In turn, in the upper inset to Fig. 12, we present the separated $C^*_m(T)$ and $S^*_m(T)$ curves. We must also add that in order to separate all these humps from the magnetic heat capacity we simplified a procedure by using the same C_m vs T fitted dependence at zero field, as indicated in Eq. (16), though the overall heat capacity values at low temperature slightly decrease under magnetic field. This of course leads to some errors but does not change our drawn main conclusions. Interestingly, the temperature T^* of each hump remains unchanged under the applied magnetic field at least up to 8 T. A similar observation of the above feature can be derived also from Fig. 4(a) of Ref. 24. The fact of keeping a constant temperature of 27 can be compared with the TMR results (see Fig. 6) obtained in various strengths of magnetic fields up to 8 T. There, we observe an opposite tendency to that in $C^*_m(T)$ as to an amplitude of the TMR which negatively grows at this characteristic temperature. It would be very interesting to compare the latter TMR observation with that made under pressure (no such data exist up to now at low pressures), when it is known from various measurements that T^* goes almost to zero at 1.2 GPa. The analysis of $\gamma(0)$ in magnetic field up to 14 T has previously been done by Lashley *et al.*[55] who found a change of about 0.5 mJ/mol K^2 per 1 T. We have observed a similar drop in $\gamma(0)$ per 1 T within our measurements of UGe_2 in magnetic fields up to 5 T.

Finally, in Fig. 13 we present the temperature variation of the magnetic entropy $S_m(T)$. According to expectation the overall relative values of $S_m(T)$ decrease under magnetic field. On the other hand, as is demonstrated in the inset to this figure, when S_m taken at characteristic T_C or T_{infl} points is plotted against the magnetic field, the S_m values at these points continuously increase with increasing strengths of the magnetic field.

IV. CONCLUSIONS

Our macroscopic studies of UGe_2, such as magnetic, electrical transport, and heat capacity ones, made in the wide temperature and magnetic-field ranges have been focused on the problem of a dual character of the 5f electrons, i.e., localized and band ones (see Ref. 64 and references therein), in one

of the most often studied compounds during more than the last ten years. First of all, we find a surprisingly good agreement between the here proposed CF level scheme, calculated on the basis of the conventional one-electron approach and the angular overlap model with the temperature variations of the susceptibilities along three main crystallographic directions, and the presence of the Schottky effect. All these features were observed in the paramagnetic region. The temperature dependencies of both above quantities can be well described by assuming the U^{4+} ($5f^2$) configuration and two very close in energy singlets as the ground state. Therefore, at least in a phenomenological manner, the obtained CF results provide a very strong theoretical argument on the localized states of the $5f$ electrons in UGe_2. A predominately localized character of these $5f^2$ magnetic electrons arises also from various other experiments; among them there are, e.g., a giant magnetocrystalline anisotropy comparable with those of prominent representatives of the rare-earth compounds. Further, observed previously and in this paper is a distinct λ-type anomaly in the temperature dependence of the heat capacity as well as the magnetic entropy at T_C; in our paper this reaches a value equal to that expected for the localized system with a ground state of a CF doublet, namely $R\ln(2)$, although it is rather a pseudodublet. The next fact on the existence of the partly localization of the $5f$ electrons provides a Kondo-lattice effect. Interestingly, the picture presented above forms a fairly close behavior to that in UPd_3 which is undoubtedly regarded as a localized system. Some of the above properties could be possible to observe due to applying here a phonon reference as $ThGe_2$, which has allowed us to separate the magnetic contributions in a proper way. Unfortunately, a majority of the authors, even after microscopic deep investigations of UGe_2 by muon spin rotation (published in 2002) that provide a proof as to the above dualism, still treat these electrons in UGe_2 as being itinerant.

On the other hand, the latter results find our full support regarding a simultaneous coexistence of local electrons with another subsystem of bandlike electrons, possessing a small magnetic moment and being characterized by high-frequency fluctuations in UGe_2. This support is uniquely yielded by our investigation of the transverse magnetoresistivity (TMR). This quantity reaches at 8 T as large value as 40% at the characteristic temperature T^* where we note a maximum of TMR. Usually, the ferromagnetic order does not cause an electron scattering at low temperature. This is why at such temperatures the magnetic moments are oriented uniformly in one direction and, hence, they do not give at all such a large contribution to the magnetoresistivity. The main reason for this high value of TMR should be, as was previously proposed in Ref. 11, the coupled CDW-SDW fluctuations. The signature of the latter behavior we also find around T^* in the form of a hump with a very small magnetic entropy superimposed on a normal $C_m(T)$ curve for a ferromagnet. This scenario is contrary to that presented very recently by Hardy *et al.*[24] in their heat-capacity analysis. As we discussed on an occasion of a study of a ferromagnet similar to UGe_2,[49] as is UCu_2Si_2, due to a large inner field, any antiferromagnetic phase cannot exist as an ordered state together with the ferromagnetism and, hence, a SDW phase has not been detected so far in UGe_2, e.g., by neutron scattering.

ACKNOWLEDGMENTS

We are grateful to H. Schilder for adapting his computer program Condon and support, and to P. Fulde for his kind interest and careful reading of the manuscript.

*R.Troc@int.pan.wroc.pl

[1] A. Huxley, I. Sheikin, E. Ressouche, N. Kernavanois, D. Braithwaite, R. Calemczuk, and J. Flouquet, Phys. Rev. B **63**, 144519 (2001).
[2] S. Kakani, M. L. Kalra, and S. L. Kakani, J. Supercond. Nov. Magn. **21**, 301 (2008).
[3] J. Linder, I. B. Sperstad, A. H. Nevidomskyy, M. Cuoco, and A. Sudbø, Phys. Rev. B **77**, 184511 (2008).
[4] G. Zwicknagl and P. Fulde, J. Phys.: Condens. Matter **15**, S1911 (2003).
[5] A. Yaouanc, P. Dalmas de Réotier, P. C. M. Gubbens, C. T. Kaiser, A. A. Menovsky, M. Mihalik, and S. P. Cottrell, Phys. Rev. Lett. **89**, 147001 (2002).
[6] S. Sakarya, P. C. M. Gubbens, A. Y. Yaouanc, P. D. de Réotier, D. Andreica, A. Amato, U. Zimmermann, N. H. van Dijk, E. Brück, Y. Huang *et al.*, Phys. Rev. B **81**, 024429 (2010).
[7] S. S. Saxena, P. Argawal, K. Ahilan, F. M. Grosche, R. K. W. Haselwimmer, M. J. Steiner, E. Pugh, I. R. Walker, S. R. Julian, P. Monthoux *et al.*, Nature (London) **406**, 587 (2000).
[8] G. Oomi, Y. Kagayama, and Y. Ōnuki, J. Alloys Compd. **271–273**, 482 (1998).
[9] G. Oomi, M. Ohashi, K. Nishimura, and Y. Ōnuki, J. Nucl. Sci. Technol. **Suppl. 3**, 90 (2002).
[10] K. Kuwahara, T. Sakai, M. Kohgi, Y. Haga, and Y. Ōnuki, J. Magn. Magn. Mater. **310**, 362 (2007).
[11] S. Watanabe and K. Miyake, J. Phys. Soc. Jpn. **71**, 2489 (2002).
[12] Y. Ushida, H. Nakane, T. Nishioka, G. Motoyama, S. Nakamura, and N. K. Sato, Physica C **388–389**, 525 (2003).
[13] R. Troć, Acta Phys. Pol. B **34**, 407 (2003).
[14] R. Troć, J. Magn. (Korea) **9**, 89 (2004).
[15] V. H. Tran, S. Paschen, R. Troć, M. Baenitz, and F. Steglich, Phys. Rev. B **69**, 195314 (2004).
[16] A. Pikul and R. Troć, Booklet of Abstracts of the 39 Journées des Actinides, La Grande–Motte; March 28–31, 2009, p. 170.
[17] A. Misiorek, J. Mucha, R. Troć, and B. Coqblin, J. Phys.: Condens. Matter **17**, 195314 (2005).
[18] M. Biasini and R. Troć, Phys. Rev. B **68**, 245118 (2003).
[19] M. Samsel-Czekała, M. Werwiński, A. Szajek, G. Chełkowska, and R. Troć, Intermetallics **19**, 1411 (2011).
[20] A. N. Yaresko, P. D. de Réotier, A. Y. Yaouanc, N. Kernavanois, J.-P. Sanches, A. A. Menovsky, and V. N. Antonov, J. Phys.: Condens. Matter **17**, 2443 (2005).

[21] K. G. Sandeman, G. G. Lonzarich, and A. J. Schofield, Phys. Rev. Lett. **90**, 167005 (2003).
[22] N. Aso, G. Motoyama, Y. Uwatoko, S. Ban, S. Nakamura, T. Nishioka, Y. Homma, Y. Shiokawa, K. Hirota, and N. K. Sato, Phys. Rev. B **73**, 054512 (2006).
[23] T. Sakon, S. Saito, K. Koyama, S. Awaji, I. Sato, T. Nojima, K. Watanabe, and N. K. Sato, Phys. Scr. **705**, 546 (2007).
[24] F. Hardy, C. Meingast, V. Taufour, J. Flouquet, H. von Löhneysen, R. A. Fisher, N. E. Phillips, A. Huxley, and J. C. Lashley, Phys. Rev. B **80**, 174521 (2009).
[25] J. Mulak and Z. Gajek, *The Effective Crystal Field Potential* (Elsevier, New York, 2000).
[26] A. Brown, Acta Crystallogr. **15**, 652 (1962).
[27] S. Hwang, K. J. Lin, and C. Tien, Rev. Sci. Instrum. **68**, 04 (1997).
[28] A. Menovsky, F. R. de Boer, P. H. Frings, and J. J. M. France, *in High Field Magnetism* (North-Holland, Amsterdam, 1983).
[29] N. Kernavanois, B. Grenier, A. Huxley, E. Ressouche, J. P. Sanchez, and J. Flouquet, Phys. Rev. B **64**, 174509 (2001).
[30] K. Hirohashi and K. Ueda, J. Phys. Soc. Jpn. **73**, 1576 (2004).
[31] Y. Ōnuki, I. Ukon, S. W. Yun, I. Umehara, K. Satoh, T. Fukuhara, H. Sato, S. Takayanagi, M. Shikama, and A. Ochiiai, J. Phys. Soc. Jpn. **61**, 293 (1992).
[32] A. Huxley, E. Ressouche, B. Grenier, D. Aoki, J. Flouquet, and C. Pfleiderer, J. Phys.: Condens. Matter **15**, S1945 (2003).
[33] P. Boulet, A. Daudi, M. Potel, H. Noël, G. M. Gross, G. Andre, and F. Bouree, J. Alloys Compd. **247**, 104 (1997).
[34] Z. Gajek, J. Krupa, Z. Zolnierek, E. Antic-Fidancev, and M. Lemaitre-Blaise, J. Phys.: Condens. Matter **5**, 9223 (1993).
[35] B. G. Wybourne, *Spectroscopic Properties of Rare Earths* (Interscience, New York, 1965).
[36] C. Rudowicz and J. Qin, J. Lumin. **110**, 39 (2004).
[37] C. K. Jorgensen, R. Pappalardo, and H. H. Schmidtke, J. Chem. Phys. **39**, 401 (1963).
[38] C. E. Schäffer and C. K. Jorgensen, Mol. Phys. **9**, 401 (1965).
[39] B. Figgis, *Introduction to Ligand Fields* (Interscience, New York, 1966).
[40] Z. Gajek, Phys. Rev. B **72**, 045139 (2005).
[41] The program Condon is free software, covered by the GNU General Public Licence, and is available from http://www.condon.fh-aachen.de.
[42] H. Lueken, *Magnetochemie* (Tuebner, Stuttgart, 1999).
[43] H. Schilder and H. Lueken, J. Magn. Magn. Mater. **281**, 17 (2004).
[44] H. Schilder (private communication).
[45] A. P. Pikul, D. Kaczorowski, Z. Gajek, J. Stępień-Damm, A. Ślebarski, M. Werwiński, and A. Szajek, Phys. Rev. B **81**, 174408 (2010).
[46] G. Grimvall, *The Electron-phonon Interaction in Metals* (North-Holland, Amsterdam, 1981), Vol. 16.
[47] T. Terashima, K. Enomoto, T. Konoike, M. Nishimura, S. Uji, N. Kimura, M. Endo, T. Komatsubara, H. Aoki, and K. Maezawa, Physica B: Condens. Matter **359**, 1060 (2005).
[48] B. Coqblin, Acta Phys. Pol. A **121**, 1005 (2012).
[49] R. Troć, M. Samsel-Czekała, J. Stępień-Damm, and B. Coqblin, Phys. Rev. B **85**, 224434 (2012).
[50] N. Aso, H. Nakane, G. Motoyama, N. Sato, Y. Uwatoko, T. Takeuchi, Y. Homma, Y. Shiokawa, and K. Hirota, Physica B: Condens. Matter **359**, 1051 (2005).
[51] G. Oomi, T. Kagayama, K. Nishimura, S. Yun, and Y. Ōnuki, Physica B: Condens. Matter **206**, 515 (1995).
[52] Y. Ōnuki, S. Yun, I. Ukon, I. Umehara, K. Satoh, I. Sakamoto, M. Hunt, P. Meeson, P. Probst, and M. Springford, J. Phys. Soc. Jpn. **60**, 2127 (1991).
[53] R. Troć, J. Alloys Compd. **423**, 21 (2006).
[54] R. Troć, Noël, and P. Boulet, Philos. Mag. B **82**, 805 (2002).
[55] J. Lashley, R. Fisher, J. Flouquet, F. Hardy, A. Huxley, and N. Phillips, Physica B: Condens. Matter **378**, 961 (2006).
[56] S. Raymond and A. Huxley, Phys. Rev. B **73**, 094420 (2006).
[57] M. Bouvier, P. Lethuillier, and D. Schmitt, Phys. Rev. B **43**, 13137 (1991).
[58] K. D. Schotte and U. Schotte, Phys. Lett. A **55**, 38 (1975).
[59] K. Prokeš, T. Wand, A. Andreev, M. Meissner, F. Honda, and V. Sechovskỳ, J. Alloys Compd. **460**, 47 (2008).
[60] L. de Jongh and A. Miedema, Adv. Phys. **23**, 1 (1974).
[61] T. Plackowski and D. Kaczorowski, Phys. Rev. B **72**, 224407 (2005).
[62] E. Colineau, F. Wastin, J. Sanchez, and J. Rebizant, J. Phys.: Condens. Matter **20**, 075207 (2008).
[63] A. Pikul, D. Kaczorowski, H. Michor, P. Rogl, E. Bauer, G. Hilscher, and Y. Grin, J. Phys.: Condens. Matter **15**, 8837 (2003).
[64] E. Runge, P. Fulde, D. V. Efremov, N. Hasselmann, and G. Zwicknagl, Phys. Rev. B **69**, 155110 (2004).